NANO · MICRO small
www.small-journal.com

# Atomic Layer Deposition of Metal Oxide on Nanocellulose for Enabling Microscopic Characterization of Polymer Nanocomposites

*Athanasia A. Septevani, David A. C. Evans, Alireza Hosseinmardi, Darren J. Martin, John Simonsen, John F. Conley Jr.,* and Pratheep K. Annamalai**

**Analysis of cellulose nanocrystals (CNCs) at low volume fractions in polymer nanocomposites through conventional electron microscopy still remains a challenge due to insufficient contrast between CNCs and organic polymer matrices. Herein, a methodology for enhancing the contrast of CNC, through atomic layer deposition (ALD) of alumina ($Al_2O_3$) on CNCs is demonstrated. The metal oxide coated CNC allows clear visualization by transmission electron microscopy, when they are dispersed in water and polyol. A coating of about 6 ± 1 nm thick alumina layer on the CNC is achieved after 50 ALD cycles. This also enables the characterization of CNC dispersion/orientation (at 0.2 wt% loading) in an amorphous cellular system rigid polyurethane foam (RPUF), using backscattered electron microscopy with energy-dispersive X-ray spectroscopy. Microscopic analysis of the RPUF with alumina-coated CNC confirms that the predominant alignment of CNC occurs in a direction parallel to the foam rise.**

Nanocellulose has attracted a tremendous level of attention as a potential reinforcing and functional filler due to its unprecedented mechanical properties at low density, chemically reactive hydroxyl groups on the surface, and high surface area.[1] It has been investigated in various polymers such as polyurethane, polypropylene, polyethylene, polylactic acid, rubbers, acrylics, and epoxy in order to enhance important properties (mechanical, insulation, and thermal properties) of the final product.[2] In this regard, understanding the distribution orientation and alignment of nanocellulose, specifically the rod-like cellulose nanocrystal (CNC) in the polymer matrix is a critical characterization, not only to understand the improvement mechanism, but also to optimize the reinforcement potential of the CNC.[3]

In cellular polymer systems, micro/nanoscale fibers are known to align with the shear forces,[4] in the direction of foam rise[5] creating a highly anisotropic microstructure. Further, the alignment of the fibers usually has a larger effect on the tensile and flexural properties of the foam more than the compressive properties.[6] When the nanocomposites are made with carbon nanotubes and carbon nanofibers,[7] or silver nanowires[8] and various inorganic nanomaterials including metals, clay minerals, and other oxides,[9] the nanofillers are readily discernible from the polymer matrix using classical optical or electron microscopy. However, with CNC, because of its similar electron density to the polymer matrices, there is unfortunately an insufficient contrast between CNC and the polymer to allow direct observation of the CNC dispersion or alignment at low volume fractions using classical optical or electron microscopies.[10] The analysis of CNC dispersion or orientation has been attempted on the noncellular nanocomposites with high loading levels of CNC using optical (polarized) and electron microscopies,[2e,10,11] atomic force microscopy,[12] Raman spectroscopy,[2a,13] or X-ray scattering methods[14] but it is still a challenge at low loading (<1 wt%) and in porous/cellular systems. For example, scanning electron microscopy (SEM) could only visualize microscale agglomerates of CNC at the cross-sectional surface of the specimen.[10,15] Similarly, polarized optical microscopy has also been used to investigate orientation behavior of CNC (2 wt%) in polyvinyl alcohol[11a] and waterborne epoxy[2e,11b] but could not resolve below the microscale of aggregation. Transmission electron microscopy (TEM) was used on CNC-polyurethane nanocomposites[11c,12a] but the images could not confirm orientation and alignment of CNC at low loading levels. The difficulty to observe the CNC distribution in poly(ε-caprolactone) matrix using TEM was attributed to the staining hindrance caused by

Dr. A. A. Septevani, Dr. D. A. C. Evans, A. Hosseinmardi,
Prof. D. J. Martin, Dr. P. K. Annamalai
Australian Institute Bioengineering and Nanotechnology (AIBN)
The University of Queensland Brisbane
QLD 4072, Australia
E-mail: p.annamalai@uq.edu.au
Dr. A. A. Septevani
Indonesian Institute of Sciences
Research Center for Chemistry
Serpong, Tangerang Selatan 15314, Indonesia
Prof. J. Simonsen
Department of Wood Science and Engineering
Oregon State University
Corvallis, OR 97331, USA
Dr. J. F. Conley Jr.
School of Electrical Engineering and Computer Science
Oregon State University
Corvallis, OR 97331, USA
E-mail: John.Conley@oregonstate.edu
The ORCID identification number(s) for the author(s) of this article can be found under https://doi.org/10.1002/smll.201803439.

**DOI: 10.1002/smll.201803439**

the fact that CNCs are isolated within a highly hydrophobic matrix.[14a] An attempt to elucidate the CNC orientation using TEM was also reported by Wanasekara et al.,[13] but still CNCs were not clearly visible in the polystyrene and poly(vinyl alcohol) matrices due to the lack of contrast between nanofiller and the polymer matrix. As a result, most studies default to indirect analysis to predict CNC orientation and alignment by using dynamic mechanical analysis[11a] or other mechanical analysis methods,[14b] where the enhanced mechanical properties are postulated to arise due to alignment of the CNC.

Recently, while reporting on the reinforcement of rigid polyurethane foam (RPUF) using only 0.4 wt% CNC,[2f] we postulated that the observed improvement in physical properties (Young's modulus) in one direction, was due to the alignment of the CNC in the direction of foam rise within the cell struts similar to the improved mechanical properties observed with oriented nanofibrillated cellulose in nanopaper.[4] In order to confirm our hypothesis, we explored ways to increase the contrast (electron density difference) of CNC versus the polyurethane matrix. Given that CNC aerogel has been successfully coated with a thin layer of $Al_2O_3$ using atomic layer deposition (ALD),[16] we adapted this process to coat CNC which has allowed us to visualize the coated CNC in water dispersions, polyol dispersions, and then in RPUF by electron microscopy.

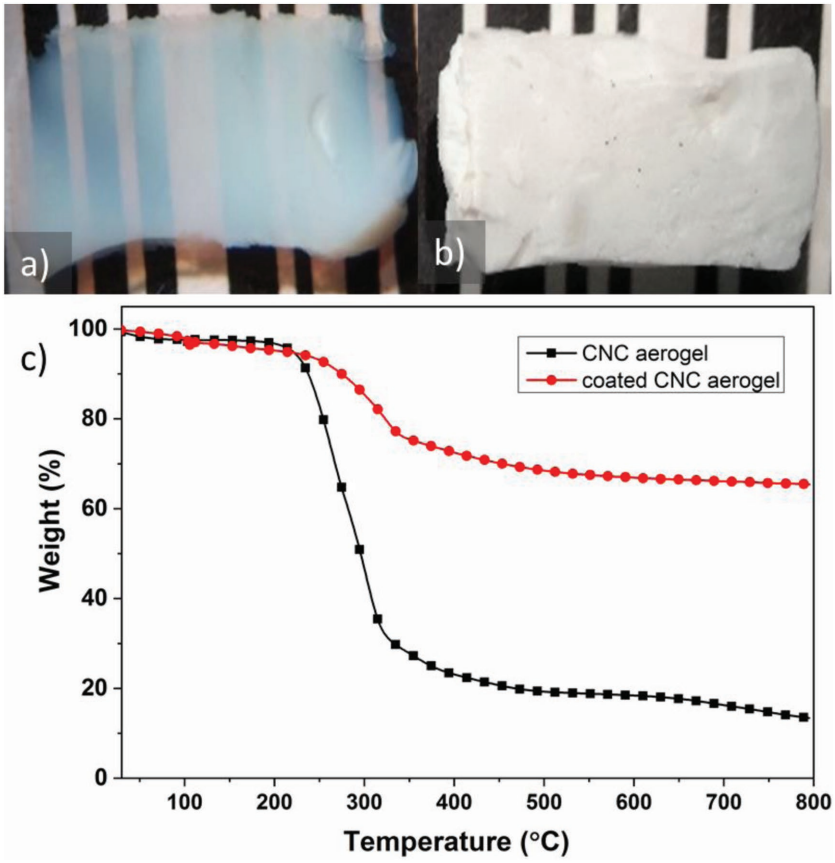


**Figure 1.** Photographs of a) CNC aerogel, b) $Al_2O_3$-coated CNC aerogel, and c) their thermogravimetric thermograms revealing deposition of inorganic material on CNCs.

Carboxylated CNC was produced through (2,2,6,6-tetramethylpiperidin-1-yl)oxyl (TEMPO) mediated oxidation at an average yield of 25 ± 5%. An aqueous dispersion of the carboxylated CNC was further processed to form CNC aerogel (**Figure 1**a) through a sol-gel method by successive solvent-exchange and supercritical drying. The thermogravimetric analysis (Figure 1c) of the CNC aerogel before and after the ALD process showed a significant improvement in thermal stability and a high residual mass (≈48% higher) for alumina ($Al_2O_3$) coated CNC aerogel supporting an effective coating of high density (3.95 g $cm^{-3}$) alumina on the CNC.[16b]

Transmission electron microscopy (TEM) was used to study the morphology and dimensions of $Al_2O_3$-coated CNC from its dispersion in a water and a polyether polyol (Voranol 446) (**Figure 2**). The dark thin layer surrounding a hollow tube indicated the $Al_2O_3$ coating on the individual CNC. The average thickness of the $Al_2O_3$ layer and CNC from TEM image at higher magnification (100k, 200 nm scale bar) of the aqueous dispersion was measured using digital image analysis (ImageJ) software with a minimum of 25 measurements along with the standard deviation. The width of the CNC (light, hollow part) was 15 ± 4 nm and which is consistent with our previous experiments on uncoated CNC.[2f] The thickness of the coated $Al_2O_3$ layer (dark, thick part) on CNC was 6 ± 1 nm, which is also consistent with the increase in the thickness of individual CNC after a typical ALD process reported previously.[16] Figure 2 (right) clearly shows that the $Al_2O_3$-coated CNC is well dispersed in Voranol 446 polyol without any damage to the CNC after crushing and high-intensity ultrasonication.

This suggests that the inorganic coating methodology may be a good approach to understanding the dispersion quality of CNC at the nanoscale level in other polymers compared to the use of polarized optical microscopy at the microscale that can only discern agglomerated nanofillers.[2e,11b] Using the dispersion of $Al_2O_3$-coated CNC in polyol, the RPUF was prepared. **Figure 3** shows the cellular structure of RPUF nanocomposites containing coated and uncoated CNC. Statistically, there was insignificant ($\alpha > 0.05$) difference between the cell sizes of the RPUF with the coated and uncoated CNC in both parallel and perpendicular to foam rise, which supports no significant difference between the coated and uncoated CNC when processed into RPUF.

Analysis of CNC alignment in RPUF using TEM is difficult due to the cellular structure. As the foam has cells with a diameter of 400–600 µm with thin cell walls, it does not have the structural rigidity to cryo-section cleanly. Attempts to fill the outer layer of foam with 20% gelatine solution in water and cryo-section resulted in sample fragmentation. Similarly, filling the outer layer of foam with Epon resin, which was then cured at 60 °C and cut at room temperature on an ultramicrotome was also unsuccessful as the sections disintegrated once they hit the water. So, in order to understand the CNC alignment in the RPUF structure,

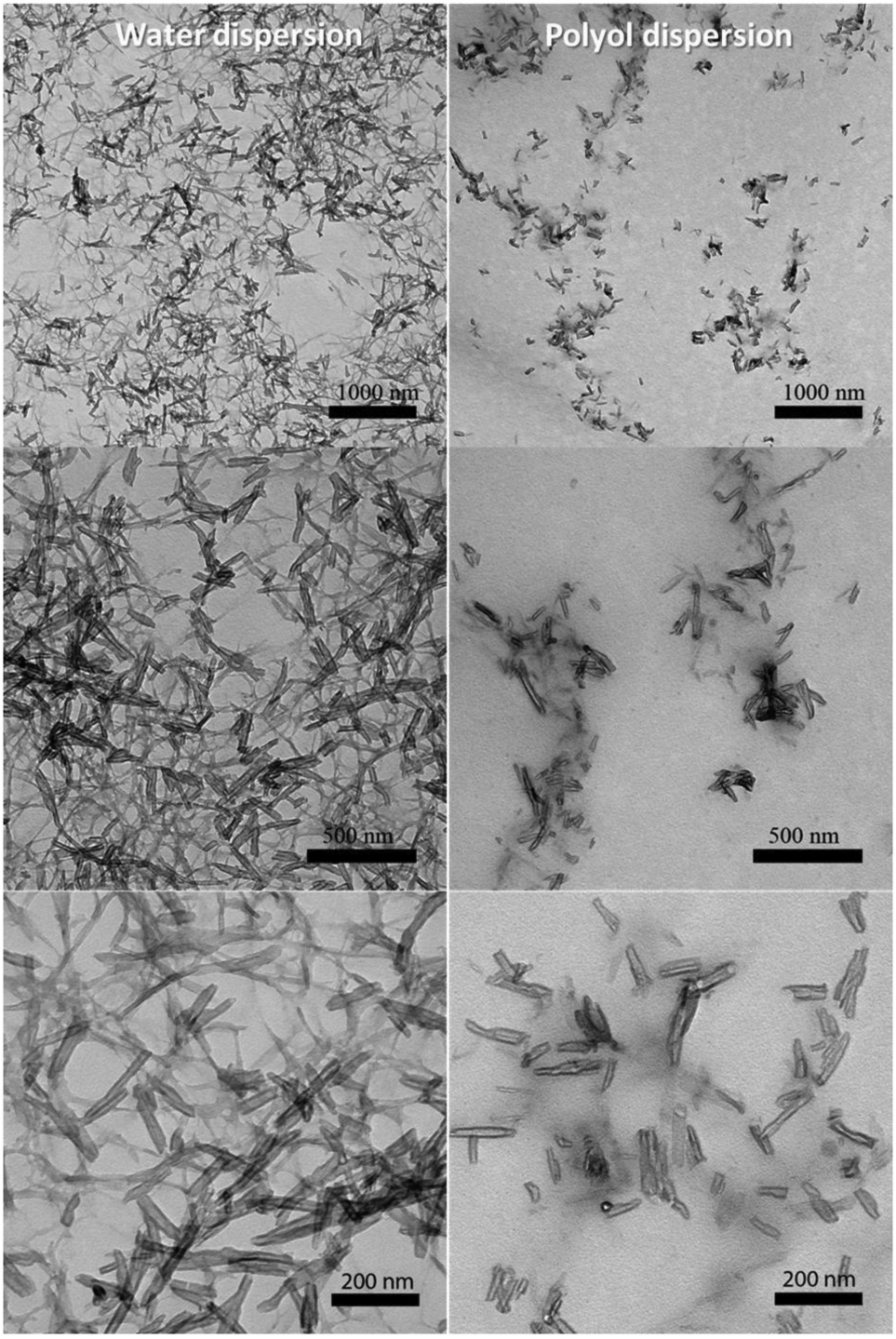


**Figure 2.** TEM images of $Al_2O_3$-coated CNC as dispersed in water (left) and in Voranol 446 polyol (right) at different magnifications.

backscattering electron microscopy (BSE) was performed both parallel and perpendicular to foam rise (**Figure 4**).

In a typical BSE analysis, the heavier element (in this case Al) appears brighter than the lighter element (carbon). The image of RPUF containing $Al_2O_3$-coated CNC parallel to foam rise (Figure 4) shows white bright spots (of CNC nanoparticles) aligned parallel to foam rise. It is confirmed that these features are rich in aluminum by energy-dispersive X-ray spectroscopy (EDX) analysis as would be expected for $Al_2O_3$-coated CNC (Figure 4). There were no such bright spots observed in the BSE image in a direction perpendicular to foam rise (Figure 4) which supports the view of CNC alignment predominantly in a direction parallel to the foam rise.

Nanoscale deposition of a metal oxide coating on individual CNC using ALD allowed direct observation of the CNC

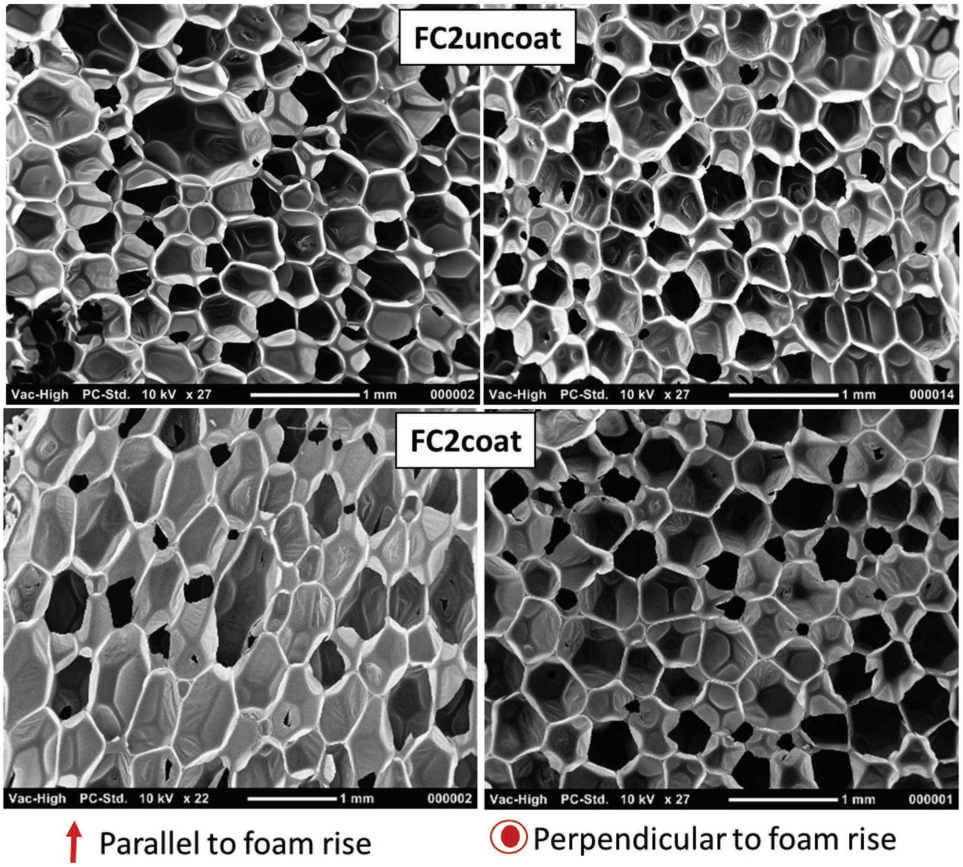


**Figure 3.** SEM images of RPUF nanocomposite containing 0.2% wt of uncoated (top) and $Al_2O_3$-coated CNC (bottom) in both parallel (left) and perpendicular (right) to foam rise.

alignment in RPUF by electron microscopy. TEM was used to study the morphology of $Al_2O_3$-coated CNC in both water and polyol dispersions. The presence of the thin layer of $Al_2O_3$ on the CNC allowed clear visualization in the polyol dispersion confirming that the CNC was well dispersed using ultrasonication. After conversion of the polyol to RPUF it was found that there were insignificant ($\alpha > 0.05$) morphology differences in the RPUF containing coated or uncoated CNC both parallel and perpendicular to foam rise. Further, BSE with EDX confirmed the existence of CNC alignment in a direction parallel to the foam rise.

## Experimental Section

Preparation of CNC aerogel and ALD of alumina layer on CNC aerogel were performed using a reported protocol.[16] First, CNC was prepared from cotton cellulose through hydrochloric acid (HCl) hydrolysis process (2.5 M HCl, 100 °C, for 30 min). Second, carboxylation was performed on the aqueous dispersion of CNC (1 at%) through a catalytic oxidation process using TEMPO agent (0.896 mmol), in the presence of sodium bromide (3.498 mmol) and sodium hypochlorite (10 mL of 10% aq. solution) in order to obtain carboxylated CNC.[17] The aqueous dispersion of carboxylated CNC (1.0–1.5%) was further processed to form CNC organogels through successive solvent-exchange sol-gel method using acetone as a miscible nonsolvent. The solvent exchange process with acetone was repeated over the course of 3–4 d, while monitoring the water content in the solvent layer. Then, the organogel was soaked in liquid $CO_2$ for about 18–24 h to remove all the acetone by slowly venting and refilling with fresh liquid $CO_2$ every 1 h. Finally, the organogel was dried using supercritical $CO_2$ at 1500 psi, 35 °C for 1 h. The vessel was then depressurized at less than 100 psi $min^{-1}$ to afford highly porous CNC aerogel. The CNC aerogel was conditioned at 125 °C for 24 h prior to the ALD process to remove all residual water or solvent. The dry CNC aerogel was then treated in an Arradiance Gemstar using trimethylaluminium (TMA) and water at 80 °C for ALD process. Each ALD cycle consisted of a sequence of (i) 1 s TMA pulse, (ii) 120 s exposure, (iii) 240 s $N_2$ purge, (iv) 0.5 s water vapor pulse, (v) 120 s exposure, and (vi) 240 s $N_2$ purge on ≈0.2 g of CNC aerogel. To ensure uniform coating of the porous aerogel, the ALD sequence in this work used an additional "soaking" step in which a throttle valve between the chamber and the pump is closed, and longer purging time to allow the reactants to fully penetrate and to be removed from the pores of the CNC, respectively. About 50 ALD cycles were performed to obtain a CNC aerogel with $Al_2O_3$ coating of ≈6 nm thickness. TEM was used to observe the morphology of $Al_2O_3$-coated CNC in both water and polyol dispersions. Thickness of the coated $Al_2O_3$ was measured from the dark thin layer surrounding the hollow tube using digital image analysis (ImageJ) software. An average of 25 measurements from a TEM image at higher magnification of the water dispersion is reported along with standard deviation. The $Al_2O_3$-coated CNC, after crushing the aerogels, was dispersed into polyol by ultrasonication following a previously reported procedure,[2f] at 20 kHz, 40 min at 80% amplitude using a probe ultrasonicator (Q500 model, QSonica). The coated CNC polyol dispersion was then converted into RPUF as previously described by Septevani et al.,[2f] by first mixing with surfactant, catalyst, a chemical blowing agent "water," and a physical blowing agent HFC-M1 (a proprietary blend of HFC245 fc and HFC365mfc) and then reacting with polymeric methylene diphenyl diisocyanate (pMDI). A control RPUF with uncoated CNC was also prepared for comparison.

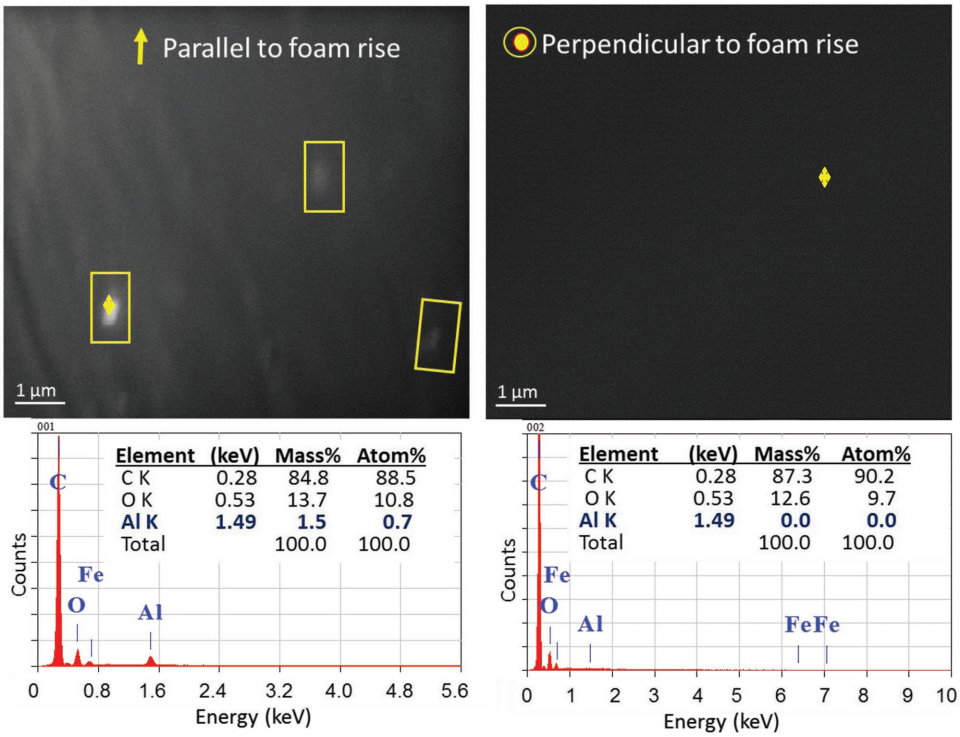


**Figure 4.** BSE images (top) and SEM-EDX pattern (bottom) of RPUF with 0.2 wt% of $Al_2O_3$-coated CNC both parallel (left) and perpendicular (right) to foam rise showing the presence of alumina on CNC in foam-rise direction (yellow diamonds represent the spots used for EDX analysis).

## Supporting Information

Supporting Information is available from the Wiley Online Library or from the author.

## Acknowledgements

A.A.S. gratefully acknowledges the financial support of an Australian Awards Scholarship by the Department of Foreign Affairs and Trade (DFAT), Australia and Graduate School International Travel Awards (GSITA) by the University of Queensland (UQ). The authors acknowledge the University of Queensland, the Australian Microscopy and Microanalysis Research Facility (AMMRF) at the Centre for Microscopy and Microanalysis (CMM) for their facilities and technical assistance. They also acknowledge the research facilities at the Oregon State University (OSU) and technical assistance by Dr. Lizandro Mazanto (OSU), Dr. Arturo Valdivia (OSU), and Dr. Isabel Morrow (UQ).

## Conflict of Interest

The authors declare no conflict of interest.

## Keywords

aerogel, atomic layer deposition, cellulose nanocrystal, microscopy, polymer nanocomposites

Received: August 24, 2018
Revised: October 3, 2018
Published online: October 16, 2018

[1] a) R. J. Moon, A. Martini, J. Nairn, J. Simonsen, J. Youngblood, *Chem. Soc. Rev.* **2011**, *40*, 3941; b) S. J. Eichhorn, A. Dufresne, M. Aranguren, N. E. Marcovich, J. R. Capadona, S. J. Rowan, C. Weder, W. Thielemans, M. Roman, S. Renneckar, W. Gindl, S. Veigel, J. Keckes, H. Yano, K. Abe, M. Nogi, A. N. Nakagaito, A. Mangalam, J. Simonsen, A. S. Benight, A. Bismarck, L. A. Berglund, T. Peijs, *J. Mater. Sci.* **2010**, *45*, 1.

[2] a) J. Mendez, P. K. Annamalai, S. J. Eichhorn, R. Rusli, S. J. Rowan, E. J. Foster, C. Weder, *Macromolecules* **2011**, *44*, 6827; b) K. N. M. Amin, N. Amiralian, P. K. Annamalai, G. Edwards, C. Chaleat, D. J. Martin, *Chem. Eng. J.* **2016**, *302*, 406; c) P. K. Annamalai, K. L. Dagnon, S. Monemian, E. J. Foster, S. J. Rowan, C. Weder, *ACS Appl. Mater. Interfaces* **2014**, *6*, 967; d) A. Hosseinmardi, P. K. Annamalai, L. Z. Wang, D. Martin, N. Amiralian, *Nanoscale* **2017**, *9*, 9510; e) S. H. Xu, N. Girouard, G. Schueneman, M. L. Shofner, J. C. Meredith, *Polymer* **2013**, *54*, 6589; f) A. A. Septevani, D. A. C. Evans, P. K. Annamalai, D. J. Martin, *Ind. Crops Prod.* **2017**, *107*, 114; g) A. A. Septevani, D. A. C. Evans, D. J. Martin, P. K. Annamalai, *Ind. Crops Prod.* **2018**, *112*, 378.

[3] a) A. Tran, W. Y. Hamad, M. J. MacLachlan, *ACS Appl. Nano Mater.* **2018**, *1*, 3098; b) M. K. Hausmann, P. A. Rühs, G. Siqueira, J. Läuger, R. Libanori, T. Zimmermann, A. R. Studart, *ACS Nano* **2018**, *12*, 6926; c) S. Chen, G. Schueneman, R. B. Pipes, J. Youngblood, R. J. Moon, *Biomacromolecules* **2014**, *15*, 3827.

[4] H. Sehaqui, N. E. Mushi, S. Morimune, M. Salajkova, T. Nishino, L. A. Berglund, *ACS Appl. Mater. Interfaces* **2012**, *4*, 1043.

[5] a) J. Shen, X. M. Han, L. J. Lee, *J. Cell. Plast.* **2006**, *42*, 105; b) M. V. Alonso, M. L. Auad, S. Nutt, *Composites, Part A* **2006**, *37*, 1952; c) H. B. Shen, S. Nutt, *Composites, Part A* **2003**, *34*, 899.

[6] a) T. C. Cotgreave, J. B. Shortall, *J. Mater. Sci.* **1977**, *12*, 708; b) Y. J. Huang, L. Vaikhanski, S. R. Nutt, *Composites, Part A* **2006**, *37*, 488.

[7] V. Dolomanova, J. C. M. Rauhe, L. R. Jensen, R. Pyrz, A. B. Timmons, *J. Cell. Plast.* **2011**, *47*, 81.

[8] a) H. J. Yun, S. J. Kim, J. H. Hwang, Y. S. Shim, S. G. Jung, Y. W. Park, B. K. Ju, *Sci. Rep.* **2016**, *6*; b) J. H. Yoo, Y. Kim, M. K. Han, S. Choi, K. Y. Song, K. C. Chung, J. M. Kim, J. Kwak, *ACS Appl. Mater. Interfaces* **2015**, *7*, 15928.
[9] a) S. H. Mir, L. A. Nagahara, T. Thundat, P. Mokarian-Tabari, H. Furukawa, A. Khosla, *J. Electrochem. Soc.* **2018**, *165*, B3137; b) S. Li, M. M. Lin, M. S. Toprak, D. K. Kim, M. Muhammed, *Nano Rev.* **2010**, *1*, 5214.
[10] M. Kaushik, C. Fraschini, G. Chauve, J.-L. Putaux, A. Moores, *The Transmission Electron Microscope: Theory and Applications*, InTech, London **2015**.
[11] a) I. Kvien, K. Oksman, *Appl. Phys. A* **2007**, *87*, 641; b) N. Girouard, G. T. Schueneman, M. L. Shofner, J. C. Meredith, *Polymer* **2015**, *68*, 111; c) A. H. Pei, J. M. Malho, J. Ruokolainen, Q. Zhou, L. A. Berglund, *Macromolecules* **2011**, *44*, 4422.
[12] a) L. Rueda, A. Saralegui, B. Fernández d'Arlas, Q. Zhou, L. A. Berglund, M. A. Corcuera, I. Mondragon, A. Eceiza, *Carbohydr. Polym.* **2013**, *92*, 751; b) A. Santamaria-Echart, L. Ugarte, C. García-Astrain, A. Arbelaiz, M. A. Corcuera, A. Eceiza, *Carbohydr. Polym.* **2016**, *151*, 1203.
[13] N. D. Wanasekara, R. P. O. Santos, C. Douch, E. Frollini, S. J. Eichhorn, *J. Mater. Sci.* **2016**, *51*, 218.
[14] a) L. G. L. Germiniani, L. C. E. da Silva, T. S. Plivelic, M. C. Gonçalves, *J. Mater. Sci.* **2018**, https://doi.org/10.1007/s10853-018-2860-9; b) A. Osorio-Madrazo, M. Eder, M. Rueggeberg, J. K. Pandey, M. J. Harrington, Y. Nishiyama, J.-L. Putaux, C. Rochas, I. Burgert, *Biomacromolecules* **2012**, *13*, 850.
[15] X. D. Cao, Y. Habibi, L. A. Lucia, *J. Mater. Chem.* **2009**, *19*, 7137.
[16] a) C. Buesch, S. W. Smith, P. Eschbach, J. F. Conley Jr., J. Simonsen, *Biomacromolecules* **2016**, *17*, 2956; b) S. W. Smith, C. Buesch, D. J. Matthews, J. Simonsen, J. F. Conley, *J. Vac. Sci. Technol., A* **2014**, *32*, 041508.
[17] F. Rafieian, J. Simonsen, *Cellulose* **2014**, *21*, 4167.